Inorg. Chem. **2004**, *43*, 1517−1529

The Solution Structure of Rhombic Lanthanide Complexes Analyzed with a Model-Free and Crystal-Field Independent Paramagnetic NMR Method: Application to Nonaxial Trimetallic Complexes $[Ln_xLu_{3-x}(TACI\text{-}3H)_2(H_2O)_6]^{3+}$ ($x = 1$–3)

Nadjet Ouali,[†] Jean-Pierre Rivera,[†] David Chapon,[‡] Pascale Delangle,*[,‡] and Claude Piguet*[,†]

Department of Inorganic, Analytical and Applied Chemistry, University of Geneva, 30 Quai E. Ansermet, CH-1211 Geneva 4, Switzerland, and Laboratoire de Reconnaissance Ionique, Service de Chimie Inorganique et Biologique, CEA/DSM/Département de Recherche Fondamentale sur la Matière Condensée, CEA-Grenoble, 38054 Grenoble Cedex 9, France

Received September 16, 2003

The model-free approach has been extended with the derivation of a novel three-nuclei crystal-field independent method for investigating isostructurality in nonaxial (i.e., rhombic) complexes along the lanthanide series. Application of this technique to the heterotrimetallic sandwich complexes $[LnLu_2(TACI\text{-}3H)_2(H_2O)_6]^{3+}$, which possess a single C_{2v}-symmetrical paramagnetic center, unambiguously evidences isostructurality for Ln = Pr–Yb, while the variation of the second-rank crystal-field parameters B_0^2 and B_2^2 along the series prevents reliable structural analyses with the classical one-nucleus equation. Extension toward polymetallic magnetically noncoupled rhombic lanthanide complexes in $[Ln_2Lu(TACI\text{-}3H)_2(H_2O)_6]^{3+}$ (two paramagnetic centers with C_s microsymmetry) and $[Ln_3(TACI\text{-}3H)_2(H_2O)_6]^{3+}$ (three paramagnetic centers with C_{2v} microsymmetry) requires only minor modifications of the original three-nuclei equation. Isostructurality characterizes $[Ln_2Lu(TACI\text{-}3H)_2(H_2O)_6]^{3+}$ (Ln = Pr–Yb), while $[Ln_3(TACI\text{-}3H)_2(H_2O)_6]^{3+}$ exhibit a structural change between Eu and Tb which results from the concomitant contraction of the three metallic centers. Particular attention has been focused on (i) the stepwise increase of contact (i.e., through-bond) and pseudocontact (i.e., through-space) contributions when the number of paramagnetic centers increases, (ii) the assignment of ^{13}C resonances in the strongly paramagnetic complexes $[Ln_3(TACI\text{-}3H)_2(H_2O)_6]^{3+}$ (Ln = Tb–Yb) for which reliable T_1 measurements and $\{^1H–^{13}C\}$ correlation spectra are not accessible, and (iii) the combination of crystal-field dependent and independent methods for analyzing the paramagnetic NMR spectra of axial and nonaxial lanthanide complexes.

Introduction

Although the global electronic properties of gaseous trivalent lanthanides (Ln(III), $[Xe]4f^n$ ($n = 0-14$)) are not significantly altered upon complexation,[1] the weak crystal field produced by the donor atoms in the first coordination sphere allows an ultrafine tuning of the electronic levels in the final complexes.[2] The rational design of lanthanide-based molecular devices with predetermined optical (fluoroimmunoassays, near-infrared emitters, analytical sensors)[3] and magnetic (smart and responsive MRI contrast agents)[4] functions thus relies on the capacity of the coordination chemists to program the splitting of the metal-centered electronic levels via the specific organization of the coor-

* Corresponding authors. E-mail: Delangle@drfmc.ceng.cea.fr (P.D.); Claude.Piguet@chiam.unige.ch (C.P.).
[†] Department of Inorganic Chemistry, University of Geneva.
[‡] Laboratoire de Reconnaissance Ionique, CEA-Grenoble.

(1) (a) Kaltsoyannis, N.; Scott, P. *The f-Elements*; Oxford University Press: Oxford, 1999. (b) Bünzli, J.-C. G. In *Rare Earths*; Saez Puche, R., Caro, P., Eds.; Editorial Complutense S. A.: Madrid, 1998; pp 223−259.

(2) (a) Carnall, W. T. In *Handbook on the Physics and Chemistry of Rare Earths*; Gschneidner, K. A., Jr.; Eyring, L., Eds.; North-Holland Publishing Company: Amsterdam, 1979; pp 171−208. (b) Görller-Walrand, C.; Binnemans, K. In *Handbook on the Physics and Chemistry of Rare Earths*; Gschneidner, K. A., Jr., Eyring, L., Eds.; North-Holland Publishing Company: Amsterdam, 1996; Vol. 23, pp 121−283. (c) Porcher, P. In *Rare Earths*; Saez Puche, R., Caro, P., Eds.; Editorial Complutense S. A.: Madrid, 1998; pp 43−66. (d) Görller-Walrand, C.; Binnemans, K. In *Handbook on the Physics and Chemistry of Rare Earths*; Gschneidner, K. A., Jr., Eyring, L., Eds.; North-Holland Publishing Company: Amsterdam, 1998; Vol. 25, pp 101−264. (e) Mironov, V. S.; Galyametdinov, Y. G.; Ceulemans, A.; Görller-Walrand, C.; Binnemans, K. J. *Chem. Phys.* **2002**, *116*, 4673.

10.1021/ic035093a CCC: $27.50
Published on Web 01/14/2004

dinated ligands around Ln(III). However, the poor covalency of the Ln−ligand bonds limits structural control to weak interstrand interactions, which smoothly vary along the lanthanide series with the monotonic contraction of the ionic radii when going from Ln = La to Ln = Lu.[5] It is therefore crucial to develop efficient analytical and spectroscopic tools for (i) detecting structural changes induced by interligand constraints along the lanthanide series, (ii) extracting three-dimensional structures in solution, and (iii) establishing simple correlations between molecular structures, crystal-field parameters, and electronic properties in lanthanide complexes. Paramagnetic NMR may contribute to address these challenges since the poor delocalization of the electron spin density from the open-shell Ln(III) onto the coordinated ligands provides paramagnetic dots which affect nuclear relaxations and resonances in a predictable way.[6] The paramagnetic NMR shift ($\delta_{ij}^{\text{para}}$) of a magnetically active nucleus *i* located in the vicinity of a lanthanide center *j* (Ln = Ce−Yb) is thus easily modeled by the sum of a through-bond contact contribution (δ_{ij}^{c}) associated with the small spin delocalization (eq 1, A_i is the Fermi constant, H^0 is the applied magnetic field, γ_i is the magnetogyric ratio, and $\langle S_z\rangle_j$ is the spin expectation values tabulated for the free ions at 300 K),[7] and a through-space pseudocontact contribution (δ_{ij}^{pc}) resulting from the average dipolar interaction occurring between the electron and nuclear magnetic momenta (eq 1, $\chi_{\alpha\alpha}^j$ are the components of the molecular magnetic tensor in the principal magnetic axes system with Ln(III) located at the origin, $\chi_{zz}^j - (1/3)\text{Tr}\,\chi^j$ and $\chi_{xx}^j - \chi_{yy}^j$ are, respectively, the axial and rhombic paramagnetic anisotropies, θ_i, ϕ_i, and r_i are the internal polar coordinates, and N_A is Avogadro's number).[8]

$$\delta_{ij}^{\text{para}} = \delta_{ij}^{\text{c}} + \delta_{ij}^{\text{pc}} = \frac{A_i}{\hbar\gamma_i H^0}\langle S_z\rangle_j + \frac{1}{2N_A}\left[\left(\chi_{zz}^j - \frac{1}{3}\text{Tr}\,\chi^j\right)\left(\frac{3\cos^2\theta_i - 1}{r_i^3}\right) + (\chi_{xx}^j - \chi_{yy}^j)\left(\frac{\sin^2\theta_i \cos 2\phi_i}{r_i^3}\right)\right] \quad (1)$$

The use of standard definitions for the geometrical factors $G_i = (3\cos^2\theta_i - 1)/r_i^3$ and $H_i = (\sin^2\theta_i \cos 2\phi_i)/r_i^3$, and for the contact term $F_i = (A_i/\hbar\gamma_i H^0)$, of the nucleus *i* transforms eq 1 into its usual form eq 2 which is well-suited for investigating the solution structures of lanthanide complexes such that (i) the contact and pseudocontact contributions can be separated,[9] and (ii) the paramagnetic anisotropies are satisfyingly modeled by the high-temperature expansions proposed by Bleaney in eqs 3−4 which provide simple correlations with the second-rank crystal-field parameters B_q^2 ($kT > \Delta E_{\text{CF}}$, ΔE_{CF} being the crystal-field splitting of the lowest *J* state).[10−12]

$$\delta_{ij}^{\text{para}} = F_i\langle S_z\rangle_j + \frac{1}{2N_A}\left[\left(\chi_{zz}^j - \frac{1}{3}\text{Tr}\,\chi^j\right)G_i + (\chi_{xx}^j - \chi_{yy}^j)H_i\right] \quad (2)$$

$$\chi_{zz}^j - \frac{1}{3}\text{Tr}\,\chi^j = -\frac{\beta^2(1+p^j)\xi^j N_A}{60(kT)^2}B_0^2 \quad (3)$$

$$\chi_{xx}^j - \chi_{yy}^j = -\frac{\beta^2(1+p^j)\xi^j N_A}{60(kT)^2}\sqrt{6}B_2^2 \quad (4)$$

Substituting eqs 3−4 into eq 2 gives the classical eq 5.[6,11] The first numerical terms $C_j = -(\beta^2(1+p^j)\xi^j/120(kT)^2)$, often referred to as Bleaney's factors, only depend on the electronic $4f^n$ configurations (via ξ^j and $(1+p^j)$ which are numerical factors calculated for each $4f^n$ configuration, β is the Bohr magneton),[12] and their relative values (scaled to $C_{\text{Dy}} = -100$) have been tabulated at 300 K.[10−12]

$$\delta_{ij}^{\text{para}} = F_i\langle S_z\rangle_j - \frac{\beta^2(1+p^j)\xi^j}{120(kT)^2}[B_0^2 G_i + \sqrt{6}B_2^2 H_i] = F_i\langle S_z\rangle_j + C_j(B_0^2 G_i + \sqrt{6}B_2^2 H_i) \quad (5)$$

For complexes displaying effective axial symmetry (i.e., possessing at least a C_3 axis defined as the principal magnetic *z* axis), the rhombic paramagnetic anisotropy vanishes because $\chi_{xx}^j = \chi_{yy}^j$ (i.e. $B_2^2 = 0$ in eq 4),[2] and eq 5 reduces to $\delta_{ij}^{\text{para}} = F_i\langle S_z\rangle_j + C_j B_0^2 G_i$ which is usually transformed into the two equivalent linear forms given in eqs 6−7.[9,11]

Straight lines for plots of $\delta_{ij}^{\text{para}}/\langle S_z\rangle_j$ versus $C_j/\langle S_z\rangle_j$ (eq 6) and $\delta_{ij}^{\text{para}}/C_j$ versus $\langle S_z\rangle_j/C_j$ (eq 7) along the lanthanide series

(3) (a) Sabbatini, N.; Guardigli, M.; Lehn, J.-M. *Coord. Chem. Rev.* **1993**, *123*, 201. (b) Sabbatini, N.; Guardigli, M.; Manet, I. In *Handbook on the Physics and Chemistry of Rare Earths*; Gschneidner, K. A., Jr., Eyring, L., Eds.; Elsevier: Amsterdam, 1996; Vol. 23, pp 69−119. (c) Werts, M. H. V.; Woudenberg, R. H.; Emmerink, P. G.; van Gassel, R.; Hofstraat, J. W.; Verhoeven, J. W. *Angew. Chem., Int. Ed.* **2000**, *39*, 4542. (d) Mathis, G. In *Rare Earths*; Saez Puche, R., Caro, P., Eds.; Editorial Complutense S. A.: Madrid, 1998; pp 285−298. (e) Parker, D. *Coord. Chem. Rev.* **2000**, *205*, 109.

(4) (a) Caravan, P.; Ellison, J. J.; McMurry, T. J.; Lauffer, R. B. *Chem. Rev.* **1999**, *99*, 2293. (b) *The Chemistry of Contrast Agents in Medical Magnetic Resonance Imaging*, Merbach, A. E., Toth, E., Eds; John Wiley: London, 2001. (c) Lowe, M. P. *Aust. J. Chem.* **2002**, *55*, 551. (d) Aime, S.; Castelli, D. D.; Fedeli, F.; Terreno, E. *J. Am. Chem. Soc.* **2002**, *124*, 9364. (e) Parker, D.; Dickins, R. S.; Puschmann, H.; Crossland, C.; Howard, J. A. K. *Chem. Rev.* **2002**, *102*, 1977.

(5) (a) Choppin, G. R. In *Lanthanide Probes in Life, Chemical and Earth Sciences*; Bünzli, J.-C. G., Choppin, G. R., Eds.; Elsevier: Amsterdam, 1989; Chapter 1, pp 1−41. (b) Bünzli, J.-C. G.; Piguet, C. *Chem. Rev.* **2002**, *102*, 1897.

(6) (a) Peters, J. A.; Huskens, J.; Raber, D. J. *Prog. NMR Spectrosc.* **1996**, *28*, 283. (b) Forsberg, J. H. In *Handbook on the Physics and Chemistry of Rare Earths*; Gschneidner, K. A., Eyring, L., Eds.; Elsevier: Amsterdam, 1996; Vol. 23, Chapter 153, p 1. (c) Geraldes, C. F. G. C. In *NMR in Supramolecular Chemistry*; Pons, M., Ed.; Kluwer Academic: Amsterdam, 1999; pp 133−154.

(7) Golding, R. M.; Halton, M. P. *Aust. J. Chem.* **1972**, *25*, 2577.

(8) (a) Kemple, M. D.; Ray, B. D.; Lipkowitz, K. B.; Prendergast, F. G.; Rao, B. D. N. *J. Am. Chem. Soc.* **1988**, *110*, 8275. (b) Bertini, I.; Luchinat, C. *Coord. Chem. Rev.* **1996**, *150*, 1. (c) Bertini, I.; Luchinat, C.; Parigi, G. *Prog. Nucl. Magn. Reson. Spectrosc.* **2002**, *40*, 249.

(9) (a) Reilley, C. N.; Good, B. W.; Desreux, J. F. *Anal. Chem.* **1975**, *47*, 2110. (b) Desreux, J. F.; Reilley, C. N. *J. Am. Chem. Soc.* **1976**, *98*, 2105. (c) Reilley, C. N.; Good, B. W.; Allendoerfer, R. D. *Anal. Chem.* **1976**, *48*, 1446.

(10) (a) Bleaney, B. *J. Magn. Reson.* **1972**, *8*, 91. (b) Bleaney, B.; Dobson, C. M.; Levine, B. A.; Martin, R. B.; Williams, R. J. P.; Xavier, A. V. *J. Chem. Soc., Chem. Commun.* **1972**, 791.

(11) Piguet, C.; Geraldes, C. F. G. C. In *Handbook on the Physics and Chemistry of Rare Earths*; Gschneidner, K. A., Jr., Bünzli, J.-C. G., Pecharsky, V. K., Eds.; Elsevier Science: Amsterdam, **2003**; Vol. 33, Chapter 215, p 353.

(12) Abragam, A.; Bleaney, B. *Electron Paramagnetic Resonance of Transitions Ions*; Clarendon Press: Oxford, 1970; p 874.

$$\frac{\delta_{ij}^{\text{para}}}{\langle S_z\rangle_j} = F_i + B_0^2 G_i \frac{C_j}{\langle S_z\rangle_j} \quad (6)$$

$$\frac{\delta_{ij}^{\text{para}}}{C_j} = F_i \frac{\langle S_z\rangle_j}{C_j} + B_0^2 G_i \quad (7)$$

imply the invariance of G_i, B_0^2, and F_i, and this has been used as a criteria for isostructurality.[6,9,11] Although corrections for the minor effects of the smooth lanthanide contraction affecting G_i have been proposed by Peters,[13] the major limitation of this one-nucleus crystal-field dependent method results from the variations of B_q^2 with the contraction of the 4f orbitals[2,14] which prevent linear correlations according to eqs 6−7 within an isostructural series.[15] This limitation has been removed for axial systems with the simultaneous consideration of the NMR signals for two nuclei i and k in the same lanthanide complex. The combination of two one-nucleus equations similar to eq 6, but expressed for the nuclei i and k, respectively, allows the removal of B_0^2. Simple algebraic transformations eventually provide the linear crystal-field independent eq 8[15d] which allows the detection of reliable structural changes along the lanthanide series since plots of $\delta_{ij}^{\text{para}}/\langle S_z\rangle_j$ versus $\delta_{kj}^{\text{para}}/\langle S_z\rangle_j$ deviate from linearity when the ratio of the geometrical parameters G_i/G_k varies.[15]

$$\frac{\delta_{ij}^{\text{para}}}{\langle S_z\rangle_j} = \left(F_i - F_k \frac{G_i}{G_k}\right) + \frac{G_i}{G_k}\frac{\delta_{kj}^{\text{para}}}{\langle S_z\rangle_j} \quad (8)$$

The recent combination of the one-nucleus crystal-field dependent eqs 6−7 with the two-nuclei crystal-field independent eq 8 for analyzing the paramagnetic NMR spectra of C_4- and C_3-symmetrical lanthanide complexes has allowed a safe re-evaluation of the specific structural and electronic effects occurring along the lanthanide series (geometrical changes, variation of crystal-field parameters, variation of the Fermi constants).[11,15−17] However this approach is strictly limited to axial systems for which the paramagnetic anisotropy is characterized by a single second-rank crystal field parameter (B_0^2). For nonaxial (i.e. rhombic) lanthanide complexes possessing at most a C_2 (or S_2) axis, the rhombic paramagnetic anisotropy cannot be neglected ($B_2^2 \neq 0$ and $\chi_{xx}^j \neq \chi_{yy}^j$ in eq 4) and eqs 6−8 are inadequate. We report in this paper on the development of an analogous set of crystal-field dependent and independent equations adapted to the model-free analysis of the paramagnetic NMR data provided by rhombic lanthanide complexes. Its application to the heterotrimetallic sandwich complexes $[LnLu_2(TACI\text{-}3H)_2(H_2O)_6]^{3+}$ possessing a single paramagnetic C_{2v}-symmetrical center is described together with its extension for the analysis of NMR data obtained for the related complexes $[Ln_2Lu(TACI\text{-}3H)_2(H_2O)_6]^{3+}$ and $[Ln_3(TACI\text{-}3H)_2(H_2O)_6]^{3+}$ possessing two and three, respectively, uncoupled paramagnetic centers (Figure 1).[18,19]

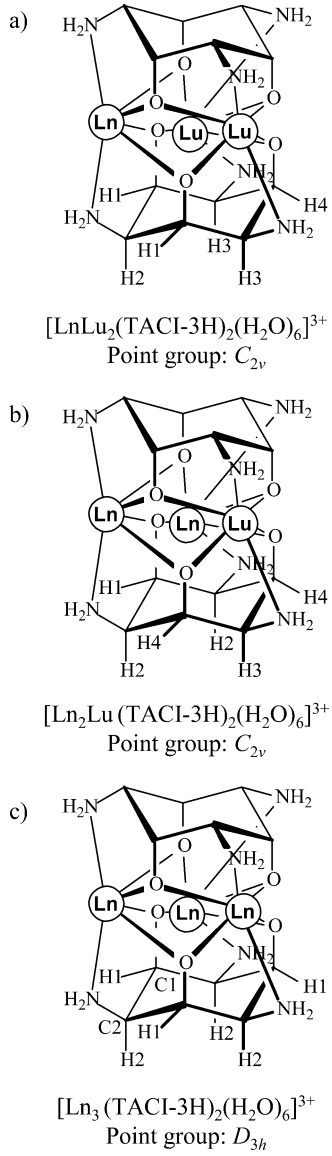

Figure 1. Schematic structures with numbering schemes for the trimetallic sandwich complexes (a) $[LnLu_2(TACI\text{-}3H)_2(H_2O)_6]^{3+}$, (b) $[Ln_2Lu(TACI\text{-}3H)_2(H_2O)_6]^{3+}$, and (c) $[Ln_3(TACI\text{-}3H)_2(H_2O)_6]^{3+}$. Each metallic site in these complexes is further coordinated by two equatorial water molecules which have been omitted for clarity.[18−19]

(13) Peters, J. A. *J. Magn. Reson.* **1986**, *68*, 240.
(14) (a) Freeman, A. J.; Watson, R. E. *Phys. Rev. B.* **1962**, *127*, 2058. (b) Hopkins, T. A.; Bolender, J. P.; Metcalf, D. H.; Richardson, F. S. *Inorg. Chem.* **1996**, *35*, 5356. (c) Hopkins, T. A.; Metcalf, D. H.; Richardson, F. S. *Inorg. Chem.* **1998**, *37*, 1401. (d) Ishikawa, N. J. *Phys. Chem. A* **2003**, *107*, 5831.
(15) (a) Reuben, J. *J. Magn. Reson.* **1982**, *50*, 233. (b) Spiliadis, S.; Pinkerton, A. A. *J. Chem. Soc., Dalton Trans.* **1982**, 1815. (c) Ren, J.; Sherry, A. D. *J. Magn. Reson.* **1996**, *B111*, 178. (d) Platas, C.; Avecilla, F.; de Blas, A.; Geraldes, C. F. G. C.; Rodriguez-Blas, T.; Adams, H.; Mahia, J. *Inorg. Chem.* **1999**, *38*, 3190. (e) Rigault, S.; Piguet, C. *J. Am. Chem. Soc.* **2000**, *122*, 9304.
(16) (a) Ren, J.; Zhang, S.; Sherry, A. D.; Geraldes, C. F. G. C. *Inorg. Chim. Acta* **2002**, *339*, 273. (b) Geraldes, C. F. G. C.; Zhang, S.; Sherry, A. D. *Bioinorg. Chem. Appl.* **2003**, *1*, 1.
(17) Ouali, N.; Bocquet, B.; Rigault, S.; Morgantini, P.-Y.; Weber, J.; Piguet, C. *Inorg. Chem.* **2002**, *41*, 1436.
(18) Chapon, D.; Delangle, P.; Lebrun, C. *J. Chem. Soc., Dalton Trans.* **2002**, 68.
(19) (a) Hedinger, R.; Ghisletta, M.; Hegetschweiler, K.; Toth, E.; Merbach, A. E.; Sessoli, R.; Gatteschi, D.; Gramlich, V. *Inorg. Chem.* **1998**, *37*, 6698. (b) Toth, E.; Helm, L.; Merbach, A. E.; Hedinger, R.; Hegetschweiler, K.; Janossy, A. *Inorg. Chem.* **1998**, *37*, 4104. (c) Chapon, D.; Husson, C.; Delangle, P.; Lebrun, C.; Vottéro, P. J. A. *J. Alloys Compd.* **2001**, *323−324*, 128.

Results and Discussion

Model-Free Crystal-Field Dependent and Independent Methods for Analyzing Monoparamagnetic Rhombic Lanthanide Complexes. The paramagnetic NMR shifts of a nucleus i (δ_{ij}^{para}) are obtained from the experimental data (δ_{ij}^{exp}) by using eq 9 if the residual signal of the solvent is taken as an internal reference (δ_i^{dia} is the diamagnetic contribution of the isostructural La, Y, or Lu complexes).[11]

$$\delta_{ij}^{para} = \delta_{ij}^{exp} - \delta_i^{dia} \tag{9}$$

Equation 5 then holds for modeling the paramagnetic NMR shifts in rhombic complexes according to Bleaney's theory (i.e., high-temperature expansion), and it can be transformed into two equivalent linear forms given in eqs 10−11, which are strictly similar to eqs 6−7 except for the introduction of a more complicated pseudocontact term $S_i = (B_0^2 G_i + \sqrt{6}\ B_2^2 H_i)$ which includes two crystal field parameters and two geometrical factors.

$$\frac{\delta_{ij}^{para}}{\langle S_z\rangle_j} = F_i + S_i\frac{C_j}{\langle S_z\rangle_j} \tag{10}$$

$$\frac{\delta_{ij}^{para}}{C_j} = F_i\frac{\langle S_z\rangle_j}{C_j} + S_i \tag{11}$$

Plots of $\delta_{ij}^{para}/\langle S_z\rangle_j$ versus $C_j/\langle S_z\rangle_j$ (eq 10) and δ_{ij}^{para}/C_j versus $\langle S_z\rangle_j/C_j$ (eq 11) along an isostructural lanthanide series are expected to give straight lines if B_q^2 ($q = 0, 2$) and F_i do not vary. These criteria are identical to those established for an axial system, but the probability of a concomitant invariance of two crystal-field parameters for rhombic systems along an isostructural lanthanide series is faint,[2,14] and reliable structural changes are difficult to address. This limitation was previously recognized by Reuben and Elgavish[20] who used the experimental solid-state magnetic susceptibility tensors obtained for [Ln(dipivaloylmethane)$_3$(4-picoline)$_2$] (Ln = Pr−Yb)[21] for computing two novel sets of axial $K_j^{axial} = \alpha(\chi_{zz}^j - 1/3\ \mathrm{Tr}\ \chi^j)$ and rhombic $K_j^{rhombic} = \beta(\chi_{xx}^j - \chi_{yy}^j)$ factors scaled to $K_{Dy}^{axial} = -100$ (α and β are arbitrary proportionality constants). Interestingly, K_j^{axial} values match the original Bleaney's factors C_j in complete agreement with eq 3 (B_0^2 is invariant for these complexes), but significant deviations are observed for $K_j^{rhombic}$ which suggest that eq 4 is not valid because (i) B_2^2 values vary along the series and/or (ii) high-temperature Bleaney's expansion is inadequate. The latter assumption is ruled out by the recent experimental determination of the axial and rhombic magnetic anisotropies in well-defined D_2-symmetrical macrocyclic lanthanide complexes which show good correlations between K_j^{axial} and C_j, and between $K_j^{rhombic}$ and C_j.[22] This eventually confirms that (i) eqs 3−4 are acceptable approximations for axial and rhombic anisotropies, respectively, and (ii) significant deviations of paramagnetic anisotropies from theoretical Bleaney's factors (C_j) for isostructural complexes along the lanthanide series can be assigned to variations of the crystal-field parameters.[22] In this context, an efficient tool for testing isostructurality in rhombic complexes requires a novel equation which does not depend on B_0^2 and B_2^2. This can be obtained by the simultaneous observation of the NMR signals of three different nuclei i, k, and l in a rhombic complex of a paramagnetic lanthanide j. Three equations similar to eq 5 (for i, k, and l, respectively) can be combined in order to remove the two parameters B_0^2 and B_2^2, thus leading, after tedious algebraic transformations, to the novel rhombic crystal-field independent eq 12.[23] The factors B_{ikl}, C_{ikl}, and D_{ikl} are given in eqs 13−16, and it is worth noting that an analogous mathematical treatment has been previously reported for the derivation of a crystal-field independent method in axial homotrimetallic complexes possessing two different metallic sites.[24]

$$\frac{\delta_{ij}^{para}}{\langle S_z\rangle_j} = B_{ikl} + C_{ikl}\frac{\delta_{kj}^{para}}{\langle S_z\rangle_j} + D_{ikl}\frac{\delta_{lj}^{para}}{\langle S_z\rangle_j} \tag{12}$$

$$B_{ikl} = F_i - F_k C_{ikl} - F_l D_{ikl} \tag{13}$$

$$C_{ikl} = R_{ik}\left(\frac{G_i - G_l R_{il}}{G_k R_{ik} - G_l R_{il}}\right) \tag{14}$$

$$D_{ikl} = -R_{il}\left(\frac{G_i - G_k R_{ik}}{G_k R_{ik} - G_l R_{il}}\right) \tag{15}$$

$$R_{uv} = \left(\frac{H_u}{H_v}\right) \tag{16}$$

Equation 12 corresponds to the equation of a plane perpendicular to the vector (1, $-C_{ikl}$, $-D_{ikl}$) and separated by a distance B_{ikl} from the origin in a homogeneous 3D space in which ($\delta_{ij}^{para}/\langle S_z\rangle_j$), ($\delta_{kj}^{para}/\langle S_z\rangle_j$), and ($\delta_{lj}^{para}/\langle S_z\rangle_j$) define the orthogonal x, y, and z directions. Since the structural factors C_{ikl} and D_{ikl} are complicated nonlinear combinations of the geometrical factors G_i, G_k, G_l, H_i, H_k, H_l, any deviation of the triplets (($\delta_{ij}^{para}/\langle S_z\rangle_j$), ($\delta_{kj}^{para}/\langle S_z\rangle_j$), ($\delta_{lj}^{para}/\langle S_z\rangle_j$)) from the plane defined by eq 12 along the lanthanide series implies a structural change. This criteria is closely related to the deviation of the doublets (($\delta_{ij}^{para}/\langle S_z\rangle_j$), ($\delta_{kj}^{para}/\langle S_z\rangle_j$)) from the straight line defined by eq 8 in axial complexes, which is diagnostic for a structural change.[15] The variation of the B_{ikl} factor is more difficult to interpret since the contact terms F_i, F_k, and F_l and the structural factors C_{ikl} and D_{ikl} are involved. Consequently, a translation of the plane along the lanthanide series cannot be systematically assigned to a structural change because the variation of the Fermi constants is sufficient for affecting B_{ikl} without changing C_{ikl} and D_{ikl}

(20) Reuben, J.; Elgavish, G. A. *J. Magn. Reson.* **1980**, *39*, 421.
(21) Horrocks, W. deW., Jr.; Sipe, J. P. *Science* **1972**, *177*, 994.
(22) Valencia, L.; Martinez, J.; Macias, A.; Bastida, R.; Carvalho, R. A.; Geraldes, C. F. G. C. *Inorg. Chem.* **2002**, *41*, 5300.

(23) Equations 12−16 can be combined and expressed in a simpler mathematical form by using a vectorial product: $(\delta_{ij}^{para}/\langle S_z\rangle_j) = (1/m_i)(m_i F_i + m_k F_k + m_l F_l - m_k(\delta_{kj}^{para}/\langle S_z\rangle_j) - m_l(\delta_{lj}^{para}/\langle S_z\rangle_j))$ in which $\vec{m} = (m_i, m_k, m_l) = \vec{G} \times \vec{H}$ ($\vec{G}$ and $\vec{H}$ are the vectors associated with the geometrical factors G_i, G_k, G_l and H_i, H_k, H_l, respectively).

(24) Ouali, N.; Rivera, J.-P.; Morgantini, P.-Y.; Weber, J.; Piguet, C. *Dalton Trans.* **2003**, 1251.

(related translations of the intercept $F_i - F_k(G_i/G_k)$ according to eq 8 within a series of isostructural monometallic axial complexes are well-documented).[11,15,25] Finally, the strict analogy between the monodimensional eq 8 characterizing axial complexes and the two-dimensional eq 12 adapted to rhombic complexes implies that a minor deviation from axiality ($B_2^2 \approx 0$), or a considerable difference in magnitude between the two crystal-field parameters ($\sqrt{6}B_2^2 \ll B_0^2$ or $\sqrt{6}B_2^2 \gg B_0^2$), should give triplets (($\delta_{ij}^{para}/\langle S_z\rangle_j$), ($\delta_{kj}^{para}/\langle S_z\rangle_j$), ($\delta_{lj}^{para}/\langle S_z\rangle_j$)) distributed approximately along a straight line within the plane defined by eq 12 (i.e., one of the pseudocontact contribution in eq 5 is negligible).

Application of the Model-Free Methods for Analyzing Isostructurality in the Monoparamagnetic Rhombic Complexes $[LnLu_2(TACI\text{-}3H)_2(H_2O)_6]^{3+}$ (Ln = Pr−Yb). Previous detailed thermodynamic and structural studies show that the solid-state structures found for $[Ln_3(TACI\text{-}3H)_2(H_2O)_6]^{3+}$ (Ln = La, Gd, Lu), in which three equivalent eight-coordinate Ln(III) species are sandwiched by two deprotonated TACI-3H ligands, are essentially maintained in solution (Figure 1c).[18,19,26] For concentrations used in NMR measurements (10^{-2}−10^{-3}M, pD = 8), the trimetallic complexes are quantitatively formed in solution, and the use of Ln/Lu pairs under stoichiometric conditions ($Ln_{tot}/TACI_{tot}$ = 3:2 and Ln_{tot} = Ln + Lu) provides mixtures containing exclusively the D_{3h}-symmetrical homotrimetallic complexes $[Ln_3(TACI\text{-}3H)_2(H_2O)_6]^{3+}$ and $[Lu_3(TACI\text{-}3H)_2(H_2O)_6]^{3+}$ and the heterotrimetallic C_{2v}-symmetrical complexes $[Ln_2Lu(TACI\text{-}3H)_2(H_2O)_6]^{3+}$ and $[LnLu_2(TACI\text{-}3H)_2(H_2O)_6]^{3+}$.[18] For the sake of simplicity, the homotrimetallic complexes will be designated by Ln_3 and Lu_3 and the heterotrimetallic species by Ln_xLu_{3-x} (x = 1−2). Since intermolecular chemical exchange is slow on the NMR time scale at RT, the four complexes provide well-separated NMR spectra (Figure 2) which can be investigated with two-dimensional correlation spectroscopies (^{1}H−^{1}H-COSY, ^{1}H−^{1}H-NOESY, and ^{1}H−^{13}C-HMQC) for Ln = Pr−Eu.[18,19] For Ln = Ce(III), partial oxidation into Ce(IV) prevents the assignment of reliable NMR data, and Ln = Sm(III) is not considered for the analysis of the NMR data because of its faint paramagnetism at 298 K.[11] Lu_3 is used as the diamagnetic reference in eq 9, and the NMR signals of H1 and H2 in this complex are assigned according to the relative electron-withdrawing inductive effects produced by the adjacent C−O and C−N bonds (C−O > C−N, Table 1).[18,19]

For the monoparamagnetic complexes $LnLu_2$, we systematically observe four ^{1}H NMR signals (H1−H4) in agreement with C_{2v} symmetry (Figure 1a), and assignment is based on the nuclear relaxation induced by the electron spin of the paramagnetic lanthanide metal. For fast-relaxing paramagnetic lanthanides (Ln = Ce−Yb, except Gd), the increase of the longitudinal relaxation rate $1/T_{1i}^{para} = 1/T_{1i}^{exp} - 1/T_{1i}^{dia}$ is dominated by dipolar electron−nucleus interactions modeled with eq 17 for a single paramagnetic center.[4,6,8,11]

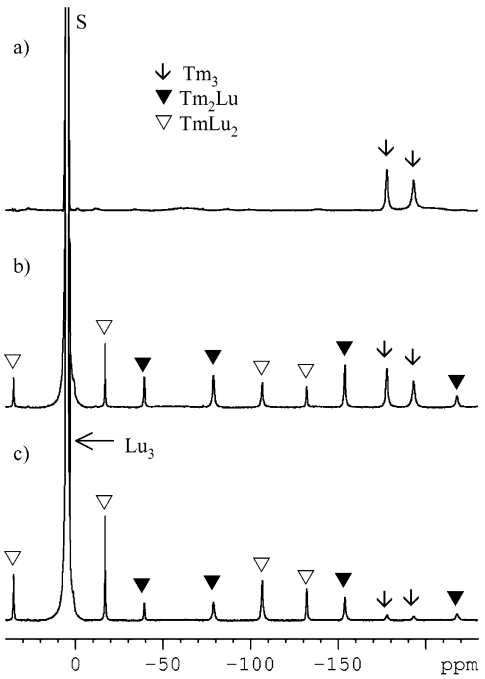

Figure 2. Part of the 400 MHz ^{1}H NMR spectra obtained for mixtures of complexes $[Tm_xLu_{3-x}(TACI\text{-}3H)_2(H_2O)_6]^{3+}$ with (a) Tm/Lu/TACI = 3:0:2, (b) Tm/Lu/TACI = 2:1:2, and (c) Tm/Lu/TACI = 1:2:2 ($TACI_{tot}$: 10^{-2} M, D_2O, pD = 8, 298 K, S = solvent).

$$\frac{1}{T_{1i}^{para}} = \frac{1}{T_{1i}^{transient}} + \frac{1}{T_{1i}^{static}} = \frac{4}{3}\left(\frac{\mu_0}{4\pi}\right)^2 \frac{\gamma_I \mu_{eff}^2 \beta^2}{r_i^6}\tau_e + \frac{6}{5}\left(\frac{\mu_0}{4\pi}\right)^2 \frac{\gamma_I^2 \mu_{eff}^4 \beta^4 H_0^2}{r_i^6 (3kT)^2}\left(\frac{\tau_r}{1+\omega_I^2\tau_r^2}\right) = E_j\left(\frac{1}{r_i^6}\right) \quad (17)$$

Since both transient and static (i.e., Curie spin) dipolar contributions depend on r_i^{-6}, we expect a linear correlation between $1/T_{1i}^{para}$ and r_i^{-6} for H1−H4 in each complex $LnLu_2$ (eq 17). Plots of $1/T_{1i}^{para}$ and r_i^{-6} obtained by using the experimental longitudinal relaxation rates (Table S1, Supporting Information) and the r_{Lu-H_i} distances measured in the crystal structure of $[Lu_3(TACI\text{-}3H)_2(H_2O)_6]^{3+}$ [26] lead to the unambiguous assignment of H1−H4 since a single permutation produces a straight line with a positive slope for each $LnLu_2$ complex (Table 1, Figure 3).

Plots of $\delta_{ij}^{para}/\langle S_z\rangle_j$ versus $C_j/\langle S_z\rangle_j$ (eq 10) and δ_{ij}^{para}/C_j versus $\langle S_z\rangle_j/C_j$ (eq 11) show significant deviations from linearity between Eu and Tb, and two straight lines for Ln = Pr−Eu and Ln = Tb−Yb are required to satisfyingly fit the ^{1}H NMR data although some residual dispersion characterizes plots according to eq 11 (Figure 4). Multilinear least-squares fits using eq 5 (i.e., δ_{ij}^{para} vs $\langle S_z\rangle_j$ and C_j) for H1−H4 in the two series provide contact (F_i) and pseudocontact terms (S_i) associated with satisfying Wilcott agreement factors $0.16 \le AF_i \le 0.22$ (eq 18, Table 2),[27] which can be compared with similar mathematical treatments

(25) Geraldes, C. F. G. C.; Zhang, S.; Platas, C.; Rodriguez-Blas, T.; de Blas, A.; Sherry, A. D. *J. Alloys Compd.* **2001**, *323*−*324*, 824.
(26) Chapon, D.; Morel, J.-P.; Delangle, P.; Gateau, C.; Pécaut. *Dalton Trans.* **2003**, 2745.
(27) Wilcott, M. R.; Lenkinski, R. E.; Davis, R. E. *J. Am. Chem. Soc.* **1972**, *94*, 1742.

Table 1. Experimental and Computed ^{1}H NMR Shifts (in ppm with Respect to DSS) with the Crystal-Field Dependent One-Nucleus Methods (eqs 5, 21) for $[Ln_xLu_{3-x}(TACI\text{-}3H)_2(H_2O)_6]^{3+}$ ($x = 0-3$, Ln = Pr−Yb) in D_2O at 298 K (pD = 8.0)[a]

compd	H1	H2	H3	H4	compd	H1	H2	H3	H4
$[Lu_3(TACI\text{-}3H)_2]^{3+}$	3.91	2.93	2.93	3.91	$[Pr_2Lu(TACI\text{-}3H)_2]^{3+}$	17.35	17.35	9.81	13.78
$[PrLu_2(TACI\text{-}3H)_2]^{3+}$	9.63	12.21	4.95	4.29	$[Pr_2Lu(TACI\text{-}3H)_2]^{3+\,b}$	18.05	18.12	10.19	14.20
$[PrLu_2(TACI\text{-}3H)_2]^{3+\,b}$	9.94	12.74	5.13	4.42	$[Nd_2Lu(TACI\text{-}3H)_2]^{3+}$	16.01	17.18	8.52	11.63
$[NdLu_2(TACI\text{-}3H)_2]^{3+}$	9.45	13.52	5.09	4.63	$[Nd_2Lu(TACI\text{-}3H)_2]^{3+\,b}$	13.28	14.15	7.05	9.96
$[NdLu_2(TACI\text{-}3H)_2]^{3+\,b}$	8.23	11.43	4.37	4.15	$[Eu_2Lu(TACI\text{-}3H)_2]^{3+}$	−11.63	−17.03	−3.06	−5.33
$[EuLu_2(TACI\text{-}3H)_2]^{3+}$	−3.61	−13.51	0.67	3.77	$[Eu_2Lu(TACI\text{-}3H)_2]^{3+\,b}$	−12.59	−18.09	−3.57	−5.91
$[EuLu_2(TACI\text{-}3H)_2]^{3+\,b}$	−4.04	−14.24	0.42	3.60	$[Tb_2Lu(TACI\text{-}3H)_2]^{3+}$	275.87	152.58	56.20	114.90
$[TbLu_2(TACI\text{-}3H)_2]^{3+}$	137.24	119.98	24.81	−32.04	$[Tb_2Lu(TACI\text{-}3H)_2]^{3+\,b}$	241.91	133.61	54.57	107.45
$[TbLu_2(TACI\text{-}3H)_2]^{3+\,b}$	124.17	106.50	24.13	−24.30	$[Dy_2Lu(TACI\text{-}3H)_2]^{3+}$	241.18	137.99	58.37	111.94
$[DyLu_2(TACI\text{-}3H)_2]^{3+}$	126.19	111.94	25.03	−23.24	$[Dy_2Lu(TACI\text{-}3H)_2]^{3+\,b}$	292.57	171.33	64.75	126.62
$[DyLu_2(TACI\text{-}3H)_2]^{3+\,b}$	149.33	138.84	28.75	−31.53	$[Ho_2Lu(TACI\text{-}3H)_2]^{3+}$	125.07	67.48	32.17	59.66
$[HoLu_2(TACI\text{-}3H)_2]^{3+}$	67.48	54.36	16.02	−6.65	$[Ho_2Lu(TACI\text{-}3H)_2]^{3+\,b}$	100.28	46.24	24.63	48.61
$[HoLu_2(TACI\text{-}3H)_2]^{3+\,b}$	53.03	34.88	11.40	−6.32	$[Er_2Lu(TACI\text{-}3H)_2]^{3+}$	−122.46	−99.58	−23.29	−43.27
$[ErLu_2(TACI\text{-}3H)_2]^{3+}$	−58.07	−84.75	−8.89	22.45	$[Er_2Lu(TACI\text{-}3H)_2]^{3+\,b}$	−126.30	−100.86	−22.68	−43.39
$[ErLu_2(TACI\text{-}3H)_2]^{3+\,b}$	−60.46	−87.33	−9.04	23.37	$[Tm_2Lu(TACI\text{-}3H)_2]^{3+}$	−218.21	−154.11	−39.40	−78.97
$[TmLu_2(TACI\text{-}3H)_2]^{3+}$	−106.87	−132.31	−17.02	35.06	$[Tm_2Lu(TACI\text{-}3H)_2]^{3+\,b}$	−181.99	−131.72	−34.74	−67.53
$[TmLu_2\ (TACI\text{-}3H)_2]^{3+\,b}$	−88.59	−111.86	−14.01	30.00	$[Yb_2Lu(TACI\text{-}3H)_2]^{3+}$	−47.47	−39.10	−9.66	−16.16
$[YbLu_2(TACI\text{-}3H)_2]^{3+}$	−21.97	−32.91	−3.03	10.51	$[Yb_2Lu(TACI\text{-}3H)_2]^{3+\,b}$	−72.10	−51.37	−12.53	−25.52
$[YbLu_2(TACI\text{-}3H)_2]^{3+\,b}$	−33.95	−43.22	−3.99	14.48					

	H1	H2	C1	C2
$[Lu_3(TACI\text{-}3H)_2]^{3+}$	3.91	2.93	75.50	57.00
$[Pr_3(TACI\text{-}3H)_2]^{3+}$	24.55	24.72	52.11	78.94
$[Pr_3(TACI\text{-}3H)_2]^{3+\,b}$	25.35	25.75	50.77	79.43
$[Nd_3(TACI\text{-}3H)_2]^{3+}$	19.30	21.80	30.34	69.70
$[Nd_3(TACI\text{-}3H)_2]^{3+\,b}$	16.17	17.77	35.60	67.78
$[Eu_3(TACI\text{-}3H)_2]^{3+}$	−14.46	−21.50	169.78	43.18
$[Eu_3(TACI\text{-}3H)_2]^{3+\,b}$	−15.55	−22.91	171.62	42.51
$[Tb_3(TACI\text{-}3H)_2]^{3+}$	264.00	193.00	652.00	452.00
$[Tb_3(TACI\text{-}3H)_2]^{3+\,b}$	236.39	169.64	591.44	407.17
$[Dy_3(TACI\text{-}3H)_2]^{3+}$	241.00	176.00	567.00	411.00
$[Dy_3(TACI\text{-}3H)_2]^{3+\,b}$	282.14	213.62	640.15	477.78
$[Ho_3(TACI\text{-}3H)_2]^{3+}$	122.00	84.00	360.00	238.00
$[Ho_3(TACI\text{-}3H)_2]^{3+b}$	101.66	62.19	343.70	202.59
$[Er_3(TACI\text{-}3H)_2]^{3+}$	−111.00	−117.00	−6.80	−127.00
$[Er_3(TACI\text{-}3H)_2]^{3+\,b}$	−111.12	−115.99	−7.35	−121.78
$[Tm_3(TACI\text{-}3H)_2]^{3+}$	−193.00	−178.00	−147.00	−250.00
$[Tm_3(TACI\text{-}3H)_2]^{3+\,b}$	−165.40	−155.24	−126.33	−203.60
$[Yb_3(TACI\text{-}3H)_2]^{3+}$	−42.30	−45.80	−29.60	4.20
$[Yb_3(TACI\text{-}3H)_2]^{3+\,b}$	−65.61	−61.10	−11.69	−49.86

[a] Sm(III) is not considered because of its faint paramagnetism. [b] Chemical shifts calculated with eqs 5, 21 and F_i^{tot} and S_i^{tot} collected in Table 2.

previously reported for $[Ln(dipicolinate)_3]^{3-}$ ($0.05 \le AF_i \le 0.22$)[17] and for homotrimetallic helicates ($0.01 \le AF_i \le 0.18$).[24]

$$AF_i = \sqrt{\frac{\sum_j (\delta_{ij}^{exp} - \delta_{ij}^{calc})^2}{\sum_j (\delta_{ij}^{exp})^2}} \qquad (18)$$

The absolute values of the contact terms decrease in the order $|F_{H2}| > |F_{H1}| \gg |F_{H3}| \approx |F_{H4}|$ (Table 2) in agreement with increasing topologic Ln−H_i separations in the $LnLu_2$ complexes (three bonds for H1, H2; four and five bonds for H3 and H4, respectively, Figure 1a). Interestingly, $|F_{H2}| > |F_{H1}|$ points to a more efficient three-bond spin delocalization from the paramagnetic center through the softer nitrogen atom (Ln−N−C−H2) compared with the deprotonated oxygen atom in Ln−O−C−H1. This supports previous reports highlighting the unusually large spin delocalization in coordinated pyridine rings.[11,28,29] Finally, the F_i values do not significantly vary between the two series (Ln = Pr−Eu and Ln = Tb−Yb) which implies no topological change along the lanthanide series. The interpretation of the pseudocontact S_i terms is limited by their complicated dependence on geometrical and crystal-field parameters (i.e., $S_i = (B_0^2 G_i + \sqrt{6} B_2^2 H_i)$). However, we expect large S_i for the protons located close to the paramagnetic center because G_i and H_i depend on r_i^{-3}, and we indeed observe the largest absolute values for $|S_{H1}|$ ($r_{Ln-H1} = 3.79$ Å) and $|S_{H2}|$ ($r_{Ln-H2} = 4.07$ Å), while $|S_{H3}|$ ($r_{Ln-H3} = 5.15$ Å) and $|S_{H4}|$ ($r_{Ln-H4} = 5.34$ Å)[26] display weaker pseudocontact contributions. The abrupt break of S_i occurring near the middle of the lanthanide series (Table 2) cannot be a priori assigned to a structural change affecting G_i and H_i without carefully evaluating possible changes in the crystal-field parameters B_0^2 and B_2^2.[11,15]

Isostructurality has been investigated with the three-nuclei crystal-field independent eq 12. Since the structural factors C_{ikl} (eq 14) and D_{ikl} (eq 15) are complicated nonlinear

(28) Rigault, S.; Piguet, C.; Bernardinelli, G.; Hopfgartner, G. *J. Chem. Soc., Dalton Trans.* **2000**, 4587.
(29) (a) Petoud, S.; Bünzli, J.-C. G.; Renaud, F.; Piguet, C.; Schenk, K. J.; Hopfgartner, G. *Inorg. Chem.* **1997**, *36*, 5750. (b) Renaud, F.; Piguet, C.; Bernardinelli, G.; Bünzli, J.-C. G.; Hopfgartner, G. *Chem. Eur. J.* **1997**, *3*, 1646.

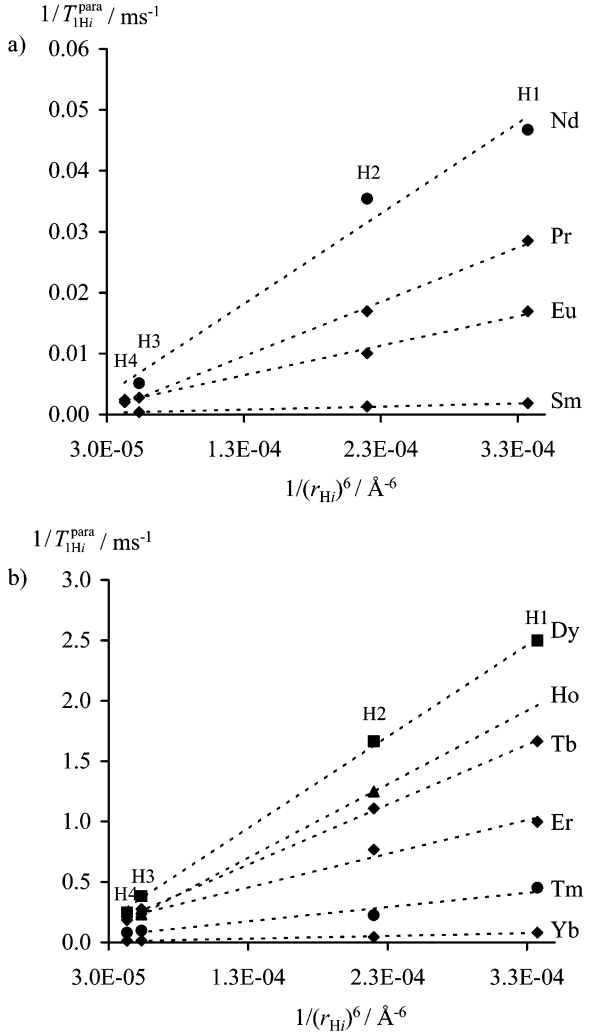

Figure 3. Plots of $1/T_1^{para}$ vs r_i^{-6} according to eq 17 for H1−H4 in $[LnLu_2(TACI\text{-}3H)_2(H_2O)_6]^{3+}$ (D_2O, pD = 8, 298 K, r_i is taken from the crystal structure of $[Lu_3(TACI\text{-}3H)_2(H_2O)_6]^{3+}$):[26] (a) Ln = Pr−Sm, (b) Ln = Tb−Yb.

functions of the geometrical parameters G_i, G_k, G_l, H_i, H_k, H_l, there is no straightforward transformation for obtaining C_{ikl} and D_{ikl} factors with a specific *ikl* ordering from the other five permutations. There are 24 ordered H*i*H*k*H*l* triplets (and 24 associated planes according to eq 12) thus required for exhaustively characterizing the solution structure of $LnLu_2$ for which the ^{1}H NMR signals of the four protons H1−H4 are available. However, the structural information contained in the four ordered combinations H*i*H*k*H*l* with $i < k < l$ is sufficient to address isostructurality.[24] Three-dimensional plots of $(\delta_{ij}^{para}/\langle S_z\rangle_j)$ versus $(\delta_{kj}^{para}/\langle S_z\rangle_j)$ and $(\delta_{lj}^{para}/\langle S_z\rangle_j)$ for the selected triplets H1H2H3, H1H2H4, H1H3H4, and H2H3H4 along the complete lanthanide series (Ln = Pr−Yb) show the experimental points to be aligned in a plane, in agreement with the existence of a single C_{2v}-symmetrical structure for $LnLu_2$ in solution (Figure 5a). The best least-squares planes characterized by B_{ikl}, C_{ikl}, and D_{ikl} (Table 3) are obtained by minimizing the sum of the square of the orthogonal distances of the experimental points $((\delta_{ij}^{para}/\langle S_z\rangle_j)$, $(\delta_{kj}^{para}/\langle S_z\rangle_j)$, $(\delta_{lj}^{para}/\langle S_z\rangle_j))$ to the plane along the lanthanide series.[30] The quality of the fit for a H*i*H*k*H*l* triplet along the series can be estimated with the average agreement

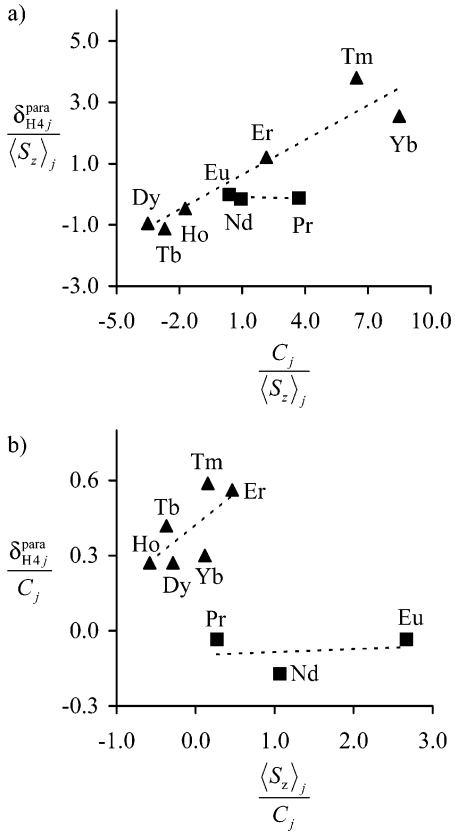

Figure 4. Plots of (a) $(\delta_{ij}^{para}/\langle S_z\rangle_j)$ vs $(C_j/\langle S_z\rangle_j)$ (eq 10) and (b) (δ_{ij}^{para}/C_j) vs $(\langle S_z\rangle_j/C_j)$ (eq 11) for H4 in $[LnLu_2(TACI\text{-}3H)_2(H_2O)_6]^{3+}$ (D_2O, pD = 8, 298 K).

factors AF_{ikl} defined in eq 19 ($||a^{obs} - a^{calc}||$ is the distance separating the experimental points $a^{obs} = ((\delta_{ij}^{para}/\langle S_z\rangle_j)$, $(\delta_{kj}^{para}/\langle S_z\rangle_j)$, $(\delta_{lj}^{para}/\langle S_z\rangle_j))$ from the related calculated points a^{calc} in the best plane).[24]

$$AF_{ikl} = \frac{1}{3}\sqrt{\frac{\sum_j ||a^{obs} - a^{calc}||^2}{\sum_j ||a^{obs}||^2}} \qquad (19)$$

The small AF_{ikl} values ($1.1 \times 10^{-3} \le AF_{ikl} \le 6.1 \times 10^{-3}$, Table 3) can be compared with those previously reported for an isostructural series in homotrimetallic helicates ($0.02 \le AF_{ikl} \le 0.17$),[24] and we conclude that $LnLu_2$ adopts a single C_{2v}-symmetrical structure in solution along the complete lanthanide series. The values of C_{ikl} and D_{ikl} are difficult to interpret and are mainly useful for comparisons with a structural model in which the principal magnetic axes are unambiguously determined. For axial systems such as the D_3-symmetrical homotrimetallic helicates previously studied with eq 12,[24] the magnetic *z* axis coincides with the 3-fold molecular axis,[11] and the required axial geometrical G_i factors are easily obtained from gas-phase models or from solid-state crystal structures.[24] For rhombic complexes, there

(30) We have used the method with Lagrangian multipliers described in ref 36 for calculating the least-squares planes (see Experimental Section).

Table 2. Computed Values for Contact ($F_i^{tot} = \sum_m F_i^m$) and Pseudocontact $S_i^{tot} = (B_0^2(\sum_m G_i^m) + \sqrt{6}B_2^2(\sum_m H_i^m))$ Terms and Agreement Factors (AF_i) for Protons and Carbons in the Complexes $[Ln_xLu_{3-x}(TACI\text{-}3H)_2(H_2O)_6]^{3+}$ ($x = 1-3$, Ln = Pr−Yb) in D_2O at 298 K ($pD = 8.0$)[a]

Ln = Pr−Eu

	$[LnLu_2(TACI\text{-}3H)_2(H_2O)_6]^{3+}$				$[Ln_2Lu(TACI\text{-}3H)_2(H_2O)_6]^{3+}$				$[Ln_3(TACI\text{-}3H)_2(H_2O)_6]^{3+}$			
	H1	H2	H3	H4	H1	H2	H3	H4	H1	H2	C1	C2
F_i^{tot}	−0.6(1)	−1.4(3)	−0.18(8)	−0.01(6)	−1.2(3)	−1.6(4)	−0.4(2)	−0.6(2)	−1.2(4)	−1.8(5)	9.1(6)	−0.6(2)
S_i^{tot}	−0.4(1)	−0.5(2)	−0.15(8)	−0.04(5)	−1.0(3)	−1.0(3)	−0.6(2)	−0.8(2)	−1.6(4)	−1.6(5)	−0.2(6)	−1.9(2)

Ln = Tb−Yb

	$[LnLu_2(TACI\text{-}3H)_2(H_2O)_6]^{3+}$				$[Ln_2Lu(TACI\text{-}3H)_2(H_2O)_6]^{3+}$				$[Ln_3(TACI\text{-}3H)_2(H_2O)_6]^{3+}$			
	H1	H2	H3	H4	H1	H2	H3	H4	H1	H2	C1	C2
F_i^{tot}	−0.7(5)	−1.8(6)	−0.14(9)	0.3(2)	−1.4(1.1)	−2.0(7)	−0.2(2)	−0.3(3)	−0.9(9)	−2.0(8)	4.2(1.4)	−1.6(1.5)
S_i^{tot}	−1.6(2)	−1.9(2)	−0.30(3)	0.44(6)	−3.3(4)	−2.2(2)	−0.68(5)	−1.3(1)	−3.1(3)	−2.7(3)	−4.5(5)	−4.7(5)
AF_i[b]	0.16	0.18	0.16	0.22	0.17	0.18	0.12	0.13	0.15	0.16	0.12	0.17

[a] F_i^{tot} and S_i^{tot} are obtained by multi-linear least-squares fits of δ_{ij}^{para} vs $\langle S_z\rangle_j$ and C_j (eqs 5, 21), and Sm(III) is not considered because of its faint paramagnetism. [b] Calculated according to eq 18.[27]

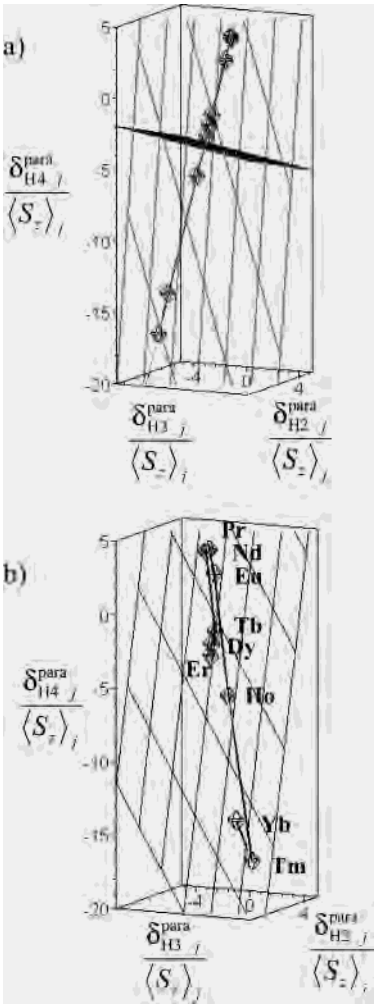

Figure 5. Three-dimensional plots of ($\delta_{ij}^{para}/\langle S_z\rangle_j$) vs ($\delta_{kj}^{para}/\langle S_z\rangle_j$) and ($\delta_{lj}^{para}/\langle S_z\rangle_j$) for H4, H2, H3 in $[LnLu_2(TACI\text{-}3H)_2(H_2O)_6]^{3+}$ (D_2O, $pD = 8$, 298 K). (a) View of the best plane from profile showing the planar arrangement of the points (rhombs are used to highlight planes orthogonal to the best plane). (b) View perpendicular to the best plane showing the location of the points within the plane (the line is only a guide for the eyes, and rhombs are used to highlight the best plane).

is no obvious correlation between the arbitrary axes fixed in the molecule and the location of the principal magnetic axes.[22,31] Therefore, any comparison with the crystal structure of $[Ln_3(TACI\text{-}3H)_2(H_2O)_6]^{3+}$ considered as a structural model

Table 3. Structural Parameters C_{ikl} and D_{ikl}, Intercepts $B_{ikl} = F_i - F_kC_{ikl} - F_lD_{ikl}$, and Agreement Factors (AF_{ikl}) Obtained from Least-Squares Planes for ($(\delta_{ij}^{para}/\langle S_z\rangle_j)$, $(\delta_{kj}^{para}/\langle S_z\rangle_j)$, $(\delta_{lj}^{para}/\langle S_z\rangle_j)$) According to Equation 12 in the Complexes $[Ln_xLu_{3-x}(TACI\text{-}3H)_2(H_2O)_6]^{3+}$ ($x = 1-3$, Ln = Pr−Yb, D_2O, pD = 8.0, 298K)[a]

$[LnLu_2(TACI\text{-}3H)_2(H_2O)_6]^{3+}$

H*i*H*k*H*l*	B_{ikl}	C_{ikl}	D_{ikl}	AF_{ikl}[b]
H1H2H3	1.03	1.09	−1.49	3.96×10^{-3}
H1H2H4	0.63	0.66	−0.81	6.02×10^{-3}
H1H3H4	0.05	2.27	−2.08	4.81×10^{-3}
H2H3H4	−0.86	3.39	−1.97	1.13×10^{-3}
	$[Ln_2Lu(TACI\text{-}3H)_2(H_2O)_6]^{3+}$			
H1H2H3	1.91	2.16	−2.46	3.71×10^{-3}
H1H2H4	9.58	9.82	−15.20	6.61×10^{-3}
H1H3H4	−0.21	−3.37	4.44	3.98×10^{-3}
H2H3H4	−0.91	−0.76	2.28	8.35×10^{-3}

$[Ln_3(TACI\text{-}3H)_2(H_2O)_6]^{3+}$ (Ln = Pr−Eu)

H/C_{ikl}	B_{ikl}	C_{ikl}	D_{ikl}	AF_{ikl}[b]
H1H2C1	0.97	1.03	−0.03	3.75×10^{-4}
H1H2C2	2.00	1.78	−0.57	4.19×10^{-4}
H1C1C2	0.67	−0.16	0.85	1.14×10^{-3}
H2C1C2	0.09	−0.23	0.69	7.39×10^{-6}
	$[Ln_3(TACI\text{-}3H)_2(H_2O)_6]^{3+}$ (Ln = Tb−Yb)			
H1H2C1	−0.96	1.00	0.17	1.11×10^{-4}
H1H2C2	1.00	1.17	−0.09	9.85×10^{-5}
H1C1C2	1.03	−0.26	0.71	4.71×10^{-5}
H2C1C2	−2.33	0.22	0.36	5.58×10^{-5}

[a] The errors on $B_{ikl}^{solution}$, $C_{ikl}^{solution}$, and $D_{ikl}^{solution}$ are typically between 1 and 5%, and Sm(III) is exceptionally considered in order to substantiate the first isostructural series in $[Ln_3(TACI\text{-}3H)_2(H_2O)_6]^{3+}$. [b] AF_{ikl} values are calculated with eq 19.

for $LnLu_2$ in solution requires the prior complete determination of the magnetic tensor in $LnLu_2$ by using the method proposed by Kemple,[8a] followed by matrix diagonalization and determination of Euler's angles tranforming the original frame into that of the principal magnetic axes system.[6,11,22,31] This sophisticated technique is well beyond the attractive model-free methods accessible to common coordination chemists, and it will not be further considered in this paper. However, the experimental B_{ikl}^{exp} parameters obtained from

(31) (a) Forsberg, J. H.; Delaney, R. M.; Zhao, Q.; Harakas, G.; Chandran, R. *Inorg. Chem.* **1995**, *34*, 3705. (b) Bertini, I.; Janik, M. B. L.; Lee, Y.-M.; Luchinat, C.; Rosato, A. *J. Am. Chem. Soc.* **2001**, *123*, 4181. (c) Di Bari, L.; Lelli, M.; Pintacuda, G.; Pescitelli, G.; Marchetti, F.; Salvadori, P. *J. Am. Chem. Soc.* **2003**, *125*, 5549.

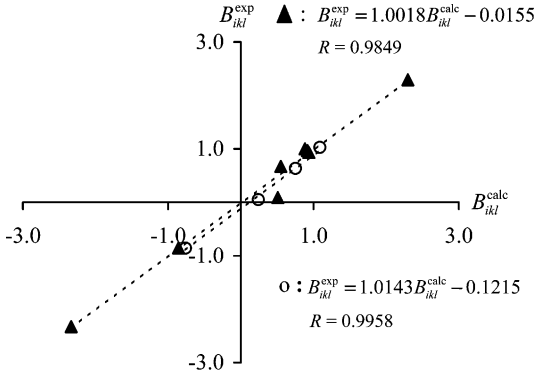

Figure 6. Plots of experimental B_{ikl}^{exp} (eq 12) for H*i*H*k*H*l* triplets as a function of B_{ikl}^{calc} calculated with eq 13 by using F_i, F_k, and F_l taken in Table 2 (see text): ○ = $[LnLu_2(TACI\text{-}3H)_2(H_2O)_6]^{3+}$ and ▲ = $[Ln_3(TACI\text{-}3H)_2(H_2O)_6]^{3+}$.

the fits of the triplets H*i*H*k*H*l* with eq 12 can be compared with those calculated B_{ikl}^{calc} with eq 13 by taking C_{ikl} and D_{ikl} from Table 3 (three-nuclei method) and F_i, F_k, and F_l from Table 2 (one-nucleus method). Since the contact terms slightly vary along the isostructural series (Table 2), the average values $F_i^{average} = 1/2(F_i^{Ln=Ce-Eu} + F_i^{Ln=Tb-Yb})$ have been used for evaluating B_{ikl}^{calc}. The excellent correlation observed between B_{ikl}^{exp} and B_{ikl}^{calc} (Figure 6) supports isostructurality for $LnLu_2$ along the complete series, and it suggests that the breaks obtained with the one-nucleus method (Figure 4) can be assigned to changes in the crystal-field parameters amplified by the abrupt increase of Bleaney's C_j factors in the second part of the series.[11,24] Finally, it is worth noting that the points $((\delta_{ij}^{para}/\langle S_z\rangle_j), (\delta_{kj}^{para}/\langle S_z\rangle_j), (\delta_{lj}^{para}/\langle S_z\rangle_j))$ only slightly deviate from a straight line within the best least-squares planes (Figure 5b), a situation which strongly contrasts with the large dispersion observed in isostructural homotrimetallic helicates (Ln = Ce−Yb).[24] This can be traced back to the two second-rank crystal-field parameters characterizing the magnetic anisotropy of the complex which are of comparable magnitude in the homotrimetallic helicates ($B_0^{2central} \approx B_0^{2terminal}$),[24] but consequently of very different size in the $LnLu_2$ complexes ($\sqrt{6}B_2^2 \ll B_0^2$ or $\sqrt{6}B_2^2 \gg B_0^2$). This translates into a weak distortion from pseudoaxiality for the $LnLu_2$ complexes which is confirmed by plots of $\delta_{ij}^{para}/\langle S_z\rangle_j$ versus $\delta_{kj}^{para}/\langle S_z\rangle_j$ for H*i*H*k* pairs according to eq 8 which poorly deviate from the straight line characterizing an isostructural series in an axial system (Figure S1, Supporting Information).

Extension of the Model-Free Crystal-Field Independent Methods for Analyzing Magnetically Noncoupled Polyparamagnetic Rhombic Lanthanide Complexes. The faint magnetic exchange observed between two Gd(III) in $[Gd_3(TACI\text{-}3H)_2(H_2O)_6]^{3+}$ ($J_{ex} = -0.092$ cm^{-1})[19b] indicates that the magnetic coupling can be neglected for analyzing ^{1}H NMR data recorded at room temperature.[32] In these conditions, the total paramagnetic shift of a nucleus *i* in a multicenter polymetallic lanthanide complex containing *n* noncoupled paramagnetic centers corresponds to the sum of the contact and pseudocontact contributions given in eq 20 such that each Ln(III) is located at the origin of a specific frame.[11,24]

$$\delta_{ij}^{para} = (\sum_{m=1}^{n} F_i^m)\langle S_z\rangle_j + C_j \sum_{m=1}^{n} (B_0^{2m} G_i^m + \sqrt{6} B_2^{2m} H_i^m) \qquad (20)$$

Since the paramagnetic centers are equivalent in $[Ln_2Lu(TACI\text{-}3H)_2(H_2O)_6]^{3+}$ (C_{2v} symmetry) and $[Ln_3(TACI\text{-}3H)_2(H_2O)_6]^{3+}$ (D_{3h} symmetry), a single set of crystal-field parameters is required,[11,24] and eq 20 reduces to eq 21 with $n = 2$ for Ln_2Lu and $n = 3$ for Ln_3. The comparison of eq 21 with eq 5 demonstrates their strict mathematic equivalence such that the original F_i, G_i, and H_i terms in eq 5 are replaced with their sum over *n* magnetic centers in eq 21. Consequently, the crystal-field independent eqs 12−16 also hold for polyparamagnetic lanthanide complexes if the original F_i, G_i, and H_i terms are replaced by their sum over *n* paramagnetic centers.

$$\delta_{ij}^{para} = (\sum_{m=1}^{n} F_i^m)\langle S_z\rangle_j + C_j (B_0{}^2 \sum_{m=1}^{n} (G_i^m) + \sqrt{6} B_2{}^2 \sum_{m=1}^{n} (H_i^m)) \qquad (21)$$

Application of the Model-Free Methods for Analyzing Isostructurality in Biparamagnetic Rhombic Complexes $[Ln_2Lu(TACI\text{-}3H)_2(H_2O)_6]^{3+}$ (Ln = Pr−Yb). The ^{1}H NMR spectra of the biparamagnetic Ln_2Lu complexes show four signals for H1−H4 (Figure 2) compatible with C_{2v} symmetry and the location of each paramagnetic center on a symmetry plane (C_s microsymmetry, Figure 1b). Extension of eq 17 for homopolymetallic paramagnetic lanthanide complexes provides eq 22,[24] and the assignment of H1−H4 given in Table 1 results from T_1 measurements for which plots of $1/T_{1i}^{para}$ versus $\sum_{m=1}^{2}(r_i^m)^{-6}$ for each Ln_2Lu complex display a straight line with a positive slope (Table S1 and Figure S2, Supporting Information).

$$\frac{1}{T_{1i}^{para}} = E_j \sum_{m=1}^{n} \left(\frac{1}{r_i^m}\right)^6 \qquad (22)$$

Plots of $\delta_{ij}^{para}/\langle S_z\rangle_j$ versus $C_j/\langle S_z\rangle_j$ (eq 10) and δ_{ij}^{para}/C_j versus $\langle S_z\rangle_j/C_j$ (eq 11) show significant deviations from linearity between Eu and Tb, and two straight lines for Ln = Pr−Eu and Ln = Tb−Yb are required to satisfyingly fit the ^{1}H NMR data as previously described for $LnLu_2$ (Figure S3, Supporting Information). Multilinear least-squares fits with eq 21 (δ_{ij}^{para} vs $\langle S_z\rangle_j$ and C_j) for H1−H4 in the two series provide contact ($F_i^{tot} = (\sum_{m=1}^{2} F_i^m)$) and pseudocontact terms ($S_i^{tot} = (B_0^2 \sum_{m=1}{}^2(G_i^m) + \sqrt{6}B_2^2 \sum_{m=1}{}^2(H_i^m))$) associated with satisfying Wilcott agreement factors $0.12 \le AF_i \le 0.18$ (eq 18, Table 2). Interestingly, the introduction of a second paramagnetic center when going from $LnLu_2$ (Figure 1a) to Ln_2Lu (Figure 1b) mainly affects $|F_{H1}^{tot}|$ and $|F_{H4}^{tot}|$, while $|F_{H2}^{tot}|$ and $|F_{H3}^{tot}|$ poorly vary. This can be traced back to the operation of two novel three-bond pathways (via the coordinated oxygen atom) allowing spin delocalization from the supplementary paramagnetic lanthanide onto H1 and H4

(32) Ishikawa, N.; Iino, T.; Kaizu, Y. *J. Am. Chem. Soc.* **2002**, *124*, 11440.

(Figure 1b). For H2 and H3, supplementary four-bond pathways become available in Ln_2Lu, but this poorly affects the contact contribution. According to the sum characterizing S_i^{tot} in eq 21, the average global increases of $|S_i^{tot}|$ observed when going from $LnLu_2$ to Ln_2Lu is not surprising since several supplementary pseudocontact shifts occurring at short distances are operating (Table 2). However, a more detailed interpretation of S_i^{tot} is precluded by (i) the complicate nonlinear variations of G_i^m and H_i^m with the internal coordinates and (ii) the absence of the location of the principal magnetic axes in Ln_2Lu.

Three-dimensional plots for H*i*H*k*H*l* triplets according to eq 12 for H1−H4 in Ln_2Lu systematically show planar arrangements along the complete series (Ln = Pr−Yb) with good agreement factors ($3.7 \times 10^{-3} \leq AF_{ikl} \leq 8.4 \times 10^{-3}$, Table 3, Figure S4, Supporting Information). This implies isostructurality for Ln_2Lu as previously established for $LnLu_2$. It is worth noting the large values of C_{ikl} and D_{ikl} found for the plane containing the H1H2H4 triplets result from its location almost parallel to the *x* direction.[24] Finally, the good correlation observed between B_{ikl}^{exp} and B_{ikl}^{calc} calculated with the contact terms collected in Table 2 (Figure S5, Supporting Information) confirms isostructurality for Ln_2Lu along the complete series. The breaks detected with the one-nucleus method (Figure S3) can be thus safely assigned to changes in the crystal-field parameters amplified by the abrupt increase of Bleaney's C_j factors as previously discussed for the $LnLu_2$ complexes.

Using the Three-Nuclei Crystal-Field Independent Method for the Assignment of ^{13}C NMR Spectra and for the Structural Analysis of the Triparamagnetic Rhombic Complexes $[Ln_3(TACI\text{-}3H)_2(H_2O)_6]^{3+}$ (Ln = Pr−Yb). The ^{1}H NMR spectra of the D_{3h}-symmetrical Ln_3 complexes (Figure 1c) exhibit only two signals corresponding to H1 and H2 which have been safely assigned through T_1 measurements according to eq 22 (i.e., the larger paramagnetic contribution $1/T_{1i}^{para}$ is ascribed to H1 for which $\sum_{m=1}^{3}(r_i^m)^{-6}$ is maximum, Table S1).[19] Plots of $\delta_{ij}^{para}/\langle S_z\rangle_j$ versus $C_j/\langle S_z\rangle_j$ (eq 10) for H1 and H2 have been originally interpreted as arising from a single isostructural series despite some minor dispersion of the points from the least-squares straight lines (Figure S6a, Supporting Information).[19c] The situation is less clear for δ_{ij}^{para}/C_j versus $\langle S_z\rangle_j/C_j$ (eq 11) which is significantly better modeled with two different series Ln = Pr−Eu and Ln = Tb−Yb in contrast with the original interpretation (Figure S6b, Supporting Information).[19c] Since only two nuclei H1 and H2 are available in Ln_3, eq 12 cannot be used for testing isostructurality around each metallic site displaying C_{2v} microsymmetry. ^{13}C NMR spectra have been thus recorded for Ln = Pr−Yb, and the observed signals have been assigned to C1 and C2 (Table 1) by using ^{1}H−^{13}C-HMQC correlation spectra for the light lanthanides Ln = Pr−Eu for which the nuclear relaxation times are long enough to allow magnetization transfer.[6b] For Ln = Tb−Yb, two broad signals are detected which cannot be assigned because of the lack of reliable T_1 measurements ($T_1 < 1$ ms) and of ^{1}H−^{13}C-HMQC correlations. Since plots $\delta_{ij}^{para}/\langle S_z\rangle_j$ versus $C_j/\langle S_z\rangle_j$ (eq 10) and δ_{ij}^{para}/C_j versus $\langle S_z\rangle_j/C_j$ (eq 11) for C1 and C2 are linear for Ln = Pr−Eu (Figure 7, full lines), we have computed with eq 21 a set of contact $F_i^{tot} = (\sum_{m=1}^{3} F_i^m)$ and pseudocontact terms $S_i^{tot} = (B_0^2 \sum_{m=1}^{3}(G_i^m) + \sqrt{6}B_2^2 \sum_{m=1}^{3}(H_i^m))$ for the light Ln(III) (Ln = Pr−Eu, Table 2). ^{13}C NMR spectra have been then predicted for each Ln_3 complex (Ln = Tb−Yb) by considering an adapted set of $\langle S_z\rangle_j$[7] and C_j[10] factors and assuming that plots of $\delta_{ij}^{para}/\langle S_z\rangle_j$ versus $C_j/\langle S_z\rangle_j$ (eq 10) and δ_{ij}^{para}/C_j versus $\langle S_z\rangle_j/C_j$ (eq 11) are linear along the complete lanthanide series.[11,15e,33] Comparisons between predicted and experimental data are only satisfying for Ln = Tb, thus leading to the assignment of C1 and C2 for this specific lanthanide which is known to act as a pivot between light and heavy Ln(III) in the model-free analyses of paramagnetic spectra.[11,15c,33] However, predictions based on the one-nucleus method fail to reproduce experimental

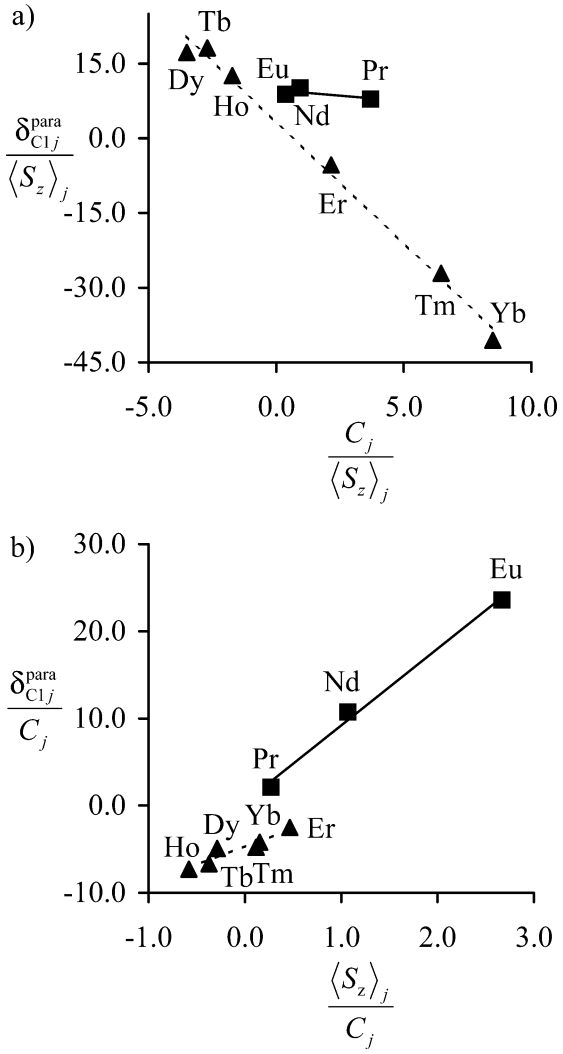

Figure 7. Plots of (a) $(\delta_{ij}^{para}/\langle S_z\rangle_j)$ vs $(C_j/\langle S_z\rangle_j)$ (eq 10) and (b) (δ_{ij}^{para}/C_j) vs $(\langle S_z\rangle_j/C_j)$ (eq 11) for C1 in $[Ln_3(TACI\text{-}3H)_2(H_2O)_6]^{3+}$ (D_2O, pD = 8, 298 K). Solid lines represent least-squares linear correlations obtained for the light lanthanides (Ln = Pr−Eu). Linear correlations for the heavy lanthanides (Ln = Tb−Yb) are shown with dotted lines.

(33) Floquet, S.; Ouali, N.; Bocquet, B.; Bernardinelli, G.; Imbert, D.; Bünzli, J.-C. G.; Hopfgartner, G.; Piguet, C. *Chem. Eur. J.* **2003**, *9*, 1860.
(34) Glasoe, P. K.; Long, F. A. *J. Phys. Chem.* **1960**, *64*, 188.

Table 4. Experimental and Computed ^{13}C NMR Shifts (in ppm with Respect to DSS) with the Crystal-Field Independent Three-Nuclei Method (eq 12) for $[Ln_3(TACI\text{-}3H)_2(H_2O)_6]^{3+}$ (Ln = Tb−Yb, D_2O, pD = 8.0, 298 K)

			one isostructural series		two isostructural series	
compd	$\delta^{exp}_{C1,j}$	$\delta^{exp}_{C2,j}$	$\delta^{calc\ a}_{C1,j}$	$\delta^{calc\ a}_{C2,j}$	$\delta^{calc\ b}_{C1,j}$	$\delta^{calc\ b}_{C2,j}$
$[Tb_3(TACI\text{-}3H)_2]^{3+}$	652	452	−1135	306	654	444
$[Dy_3(TACI\text{-}3H)_2]^{3+}$	567	411	−1051	282	593	413
$[Ho_3(TACI\text{-}3H)_2]^{3+}$	360	238	−382	183	435	213
$[Er_3(TACI\text{-}3H)_2]^{3+}$	−7	−127	291	−62	−8	−121
$[Tm_3(TACI\text{-}3H)_2]^{3+}$	−147	−250	733	−134	−149	−252
$[Yb_3(TACI\text{-}3H)_2]^{3+}$	−30	4	16	−5	−30	4

[a] Calculated with eq 12 according to a single isostructural series defined by Ln = Pr−Yb. [b] Calculated with eq 12 according to two isostructural series Ln = Pr−Eu and Ln = Tb−Yb.

data for the heavier lanthanides (Ln = Tb−Yb), which implies that a break in the crystal-field dependent eqs 10−11 occurs for C1 and C2 near the middle of the series (Figure 7).

We have then resorted to the novel three-nuclei crystal-field independent method (eq 12) for predicting the ^{13}C NMR spectra of the Ln_3 complexes with Ln = Tb−Yb. First, we have considered a single isostructural series for Ln = Pr−Yb and a preliminary set of B_{ikl}, C_{ikl}, and D_{ikl} is obtained from the fit of the two H1H2C*l* triplets according to eq 12 for Ln = Pr−Eu. Taking the accessible δ^{para}_{Hij} (Table 1) and $\langle S_z\rangle_j$ for each heavy lanthanide (Ln = Tb−Yb),[7] δ^{para}_{Cij} can be calculated with eq 12, but predictions do not agree with experimental data (Table 4). We therefore conclude that at least two isostructural series should be considered for Ln_3, and we select four strongly paramagnetic lanthanides in the second series Ln = Tb, Er, Tm, Yb for defining a second isostructural series. Although the assignment of C1 and C2 for Ln = Tb is known from prediction using the one-nucleus method, there is no a priori available attribution of the ^{13}C NMR signals in Er_3, Tm_3, and Yb_3, and we have computed B_{ikl}, C_{ikl}, D_{ikl}, and AF_{ikl} for each H1H2C*l* and H*i*C1C2 triplet (four planes) corresponding to each permutation of the ^{13}C signals observed for Ln = Tm, Er, Yb (eight possible permutations). For each permutation corresponding to a specific ^{13}C assignment, we obtain an average agreement factor considering the four triplets: $\overline{AF} = 1/4\sum_{ikl} AF_{ikl}$. A single permutation provides a satisfying agreement factor with $\overline{AF} = 6.0 \times 10^{-4}$ comparable with those found for $LnLu_2$ and Ln_2Lu, while the other permutations provide $\overline{AF} > 1.2 \times 10^{-3}$. The specific sets of B_{ikl}, C_{ikl}, and D_{ikl} parameters associated with this permutation for H1H2C*l* (*l* = 1,2) have been used for predicting the ^{13}C NMR spectra of Dy_3 and Ho_3 with eq 12 (δ^{para}_{Hij} are taken from Table 1) which indeed fit the experimental data (Table 4), and allow the complete assignment of ^{13}C resonances for the heavy Ln_3 complexes (Table 1).

The eventual thorough analysis of ^{13}C NMR data according to the crystal-field dependent eqs 10 and 11 unambiguously confirms a break near the middle of the lanthanide series which contrasts with the original treatment limited to H1 and H2,[19c] but which is in line with the existence of a structural change along the lanthanide series (Figure 7). The Wilcott agreement factors for H1, H2, C1, and C2 $0.12 \leq AF_i \leq 0.17$ (eq 18, Table 2) are comparable with those obtained for Lu_2Ln and Ln_2Lu, but slightly better than those reported for H1 and H2 calculated according to a single isostructural series ($0.18 \leq AF_i \leq 0.19$).[19c] The contact terms $F^{tot}_{H1} = (\sum^3_{m=1} F^m_{H1})$ and $F^{tot}_{H2} = (\sum^3_{m=1} F^m_{H2})$ in Ln_3 are very similar to contact terms computed in Ln_2Lu for the topologically related protons H1 and H2 (Table 2) because the introduction of the third paramagnetic center in Ln_3 brings only one supplementary four-bond pathway for spin delocalization onto H2 (Figure 1c). On the other hand, the pseudocontact terms $S^{tot}_i = (B^2_0 \sum^3_{m=1}(G^m_i) + \sqrt{6}B^2_2 \sum^3_{m=1}(H^m_i))$ are maximum for Ln_3 because of the existence of three paramagnetic centers. Three-dimensional plots of $(\delta^{para}_{ij}/\langle S_z\rangle_j)$ versus $(\delta^{para}_{kj}/\langle S_z\rangle_j)$ and $(\delta^{para}_{lj}/\langle S_z\rangle_j)$ according to eq 12 for the triplets H1H2C1, H1H2C2, H1C1C2, and H2C1C2 along the lanthanide series (Ln = Pr−Yb) show deviations from a single plane (Figure 8a) pointing to a structural change between Eu and Tb in agreement with the previous need for two different isostructural series for assigning ^{13}C NMR spectra. The use of two different planes Ln = Pr−Eu and Ln = Tb−Yb gives satisfying AF_{ikl} factors together with two sets of B_{ikl}, C_{ikl}, and D_{ikl} collected in Table 3 (Figure 8b). B^{calc}_{ikl} calculated with eq 13 (C_{ikl} and D_{ikl} taken from Table 3 and F^{tot}_i, F^{tot}_k, and F^{tot}_l from Table 2) for the two isostructural series in Ln_3 perfectly match B^{exp}_{ikl} obtained from the fitting of the triplets H*i*H*k*C*l* and H*i*C*k*C*l* (Figure 6), which eventually confirms that the structural change affects both contact terms and geometrical parameters. Although a concomitant variation of the crystal-field parameters B^2_0 and B^2_2 is expected,[2,11,14] it cannot be safely addressed with the one-nucleus crystal-field dependent eq 21 because the variations of $\sum^3_{m=1}(G^m_i)$ and $\sum^3_{m=1}(H^m_i)$ already affect S^{tot}_i.

We can safely conclude that $[Ln_3(TACI\text{-}3H)_2(H_2O)_6]^{3+}$ display a sufficient structural variation along the lanthanide series for being detected with the rhombic crystal-field independent eq 12. This contrasts with the original report based on the one-nucleus method applied to H1 and H2 (eq 10),[19b] but compensation effects between crystal-field and geometrical parameters in the pseudocontact terms S^{tot}_i are known to prevent the unambiguous detection of structural changes with crystal-field dependent methods.[17] Although the model-free methods do not allow straightforward access to the exact nature of the structural change,[11] the considerable geometrical variations induced by the lanthanide contraction in the crystal structures of $[Ln_3(TACI\text{-}3H)_2(H_2O)_6]^{3+}$ (Ln = La, Gd, Lu)[19,26] suggest parallel changes occurring in solution

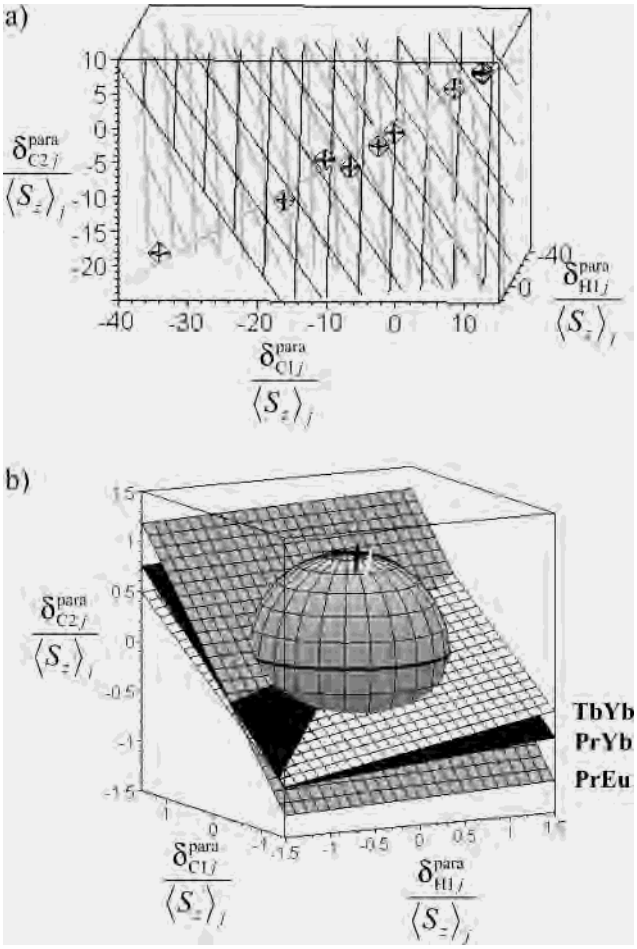

Figure 8. Three-dimensional plots of $(\delta_{ij}^{para}/\langle S_z\rangle_j)$ vs $(\delta_{kj}^{para}/\langle S_z\rangle_j)$ and $(\delta_{lj}^{para}/\langle S_z\rangle_j)$ for C2, H1, C1 in $[Ln_3(TACI\text{-}3H)_2(H_2O)_6]^{3+}$ (D_2O, pD = 8, 298 K). (a) View from profile showing the deviation of the points from a single plane (rhombs are used to highlight planes orthogonal to the best plane). (b) View of the two best planes characterizing the two different isostructural series Ln = Pr−Eu and Ln = Tb−Yb. An approximate plane obtained for a single isostructural series Ln = Pr−Yb (black) is shown for comparison (the three arrows on the sphere represents the vectors normal to the different planes).

(decrease of the separation between the facial planes defined by the alcoholate atoms of each ligand: 2.71 Å (La), 2.54 Å (Gd), 2.45 Å (Lu), and decrease of the intermetallic distances: 3.932 Å (La), 3.734 Å (Gd), 3.607 Å (Lu)). The occupancy of at least one site with a lutetium atom in the heterotrimetallic complexes $LnLu_2$ and Ln_2Lu along the lanthanide series strongly limits structural deformations, and this may explain the different behaviors observed for $LnLu_2$ and Ln_2Lu (isostructural along the complete series) and Ln_3 (structural change along the series). However, the increased sensitivity of paramagnetic shifts in axial triparamagnetic helicates has been previously invoked for rationalizing apparent structural changes in crystal-field independent equations.[24] A similar effect cannot be completely ruled out for $[Ln_3(TACI\text{-}3H)_2(H_2O)_6]^{3+}$ although the variations of the structural parameters along the lanthanide series in the solid state strongly support nonisostructurality.

Conclusion

As previously established for axial systems, the systematic variations of the crystal-field parameters B_0^2 and B_2^2 along the lanthanide series for rhombic complexes[14] prevent the use of crystal-field dependent methods for addressing structural changes according to the model-free approach. Since the number of crystal-field parameters required for modeling the molecular paramagnetic anisotropy according to Bleaney's hypothesis increases from one (B_0^2) in axial complexes to two (B_0^2 and B_2^2) in rhombic complexes, the dimensionality of the crystal-field independent equations concomitantly increases from one dimension (a straight line defined by eq 8 for axial complexes) to two dimensions (a plane defined by eq 12 for rhombic complexes). Except for this mathematical expansion, the analysis of the paramagnetic NMR data is similar, and the extension toward magnetically noncoupled polymetallic lanthanide complexes brings no drastic complication. Application of the novel rhombic crystal-field independent method to the sandwich complexes $[Ln_xLu_{3-x}(TACI\text{-}3H)_2(H_2O)_6]^{3+}$ exhibiting C_{2v} ($x = 1, 3$) or C_s ($x = 2$) microsymmetries for the paramagnetic centers demonstrates isostructurality for the heterotrimetallic complexes along the complete lanthanide series, while a significant structural variation occurs for the homotrimetallic analogues. Interestingly, the experimental points $((\delta_{ij}^{para}/\langle S_z\rangle_j), (\delta_{kj}^{para}/\langle S_z\rangle_j), (\delta_{lj}^{para}/\langle S_z\rangle_j))$ defining the isostructural plane according to eq 12 are systematically poorly dispersed around a straight line for all complexes, thus pointing to second-rank crystal-field parameters in Ln_xLu_{3-x} which display significantly different magnitudes ($\sqrt{6}B_2^2 \ll B_0^2$ or $\sqrt{6}B_2^2 \gg B_0^2$). The origin of the large discrepancy between B_0^2 and B_2^2 in Ln_xLu_{3-x} is difficult to address, but a thorough analysis of the crystal structures of $[Ln_3(TACI\text{-}3H)_2(H_2O)_6]^{3+}$ shows that the metallic sites only slightly deviate from 3-fold symmetry since they can be described as bicapped trigonal prismatic sites (the coordinated oxygen atoms define the trigonal faces of the prism and the nitrogen atoms cap two rectangular faces, Figure 9).[19,26] Theoretical PCEM calculations (PCEM = point charge electrostatic model)[2a] show that the removal of one capping atom when going from an ideal tricapped trigonal prism (D_{3h} symmetry: $B_0^2 \neq 0$ if $\theta \neq 45°$ and $B_2^2 = 0$)[2a] to a bicapped trigonal prism (C_{2v} symmetry: $B_0^2 \neq 0$ and $B_2^2 \neq 0$) produces (i) only weak distortion from axiality and (ii) limited magnetic anisotropies,[2e] two predictions which match the weak "rhombic" distortion observed by paramagnetic NMR for Ln_xLu_{3-x}.

In conclusion, the combination of the one-nucleus crystal-field dependent (eq 5) with two-nuclei crystal-field independent (eq 8, axial systems) and three-nuclei crystal-field independent (eq 12, rhombic systems) methods provides a complete and efficient tool for safely analyzing paramagnetic NMR spectra of lanthanide coordination complexes and for detecting structural changes induced by the lanthanide contraction without resorting to structural models. This point is crucial for the fast screening and evaluation of geometrical and electronic changes induced by weak intramolecular interstrand interactions responsible for structural programming and thermodynamic selectivities in sophisticated supramolecular lanthanide complexes.[4e,5b]

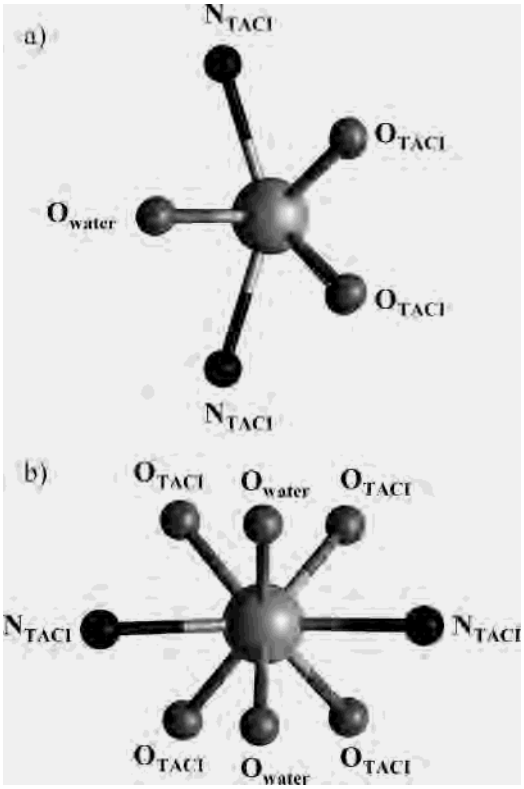

Figure 9. Perspective view of the Lu-coordination sphere in the crystal structure of $[Lu_3(TACI\text{-}3H)_2(H_2O)_6]^{3+}$ [26] highlighting the minor distortion from trigonal symmetry. (a) View along the pseudo-C_3 axis and (b) view perpendicular to the pseudo-C_3 axis.

Experimental Section

Spectroscopic Measurements. Samples for NMR spectroscopy were prepared by dissolving the ligand (10^{-2} to 10^{-3} M) and the lanthanide triflate salt in 700 μL of deuterium oxide (Euriso-top, 99.9 at. % D). The pD = 8 level was then adjusted with sodium deuteroxide solution (pD = pH + 0.41).[34] NMR spectra were recorded either on AVANCE 400 Bruker or MERCURY 400 Varian spectrometers. The methyl protons of DSS (3-(trimethylsilyl)-1-propanesufonic acid) were used as an internal reference for the ^{1}H and ^{13}C spectra recorded in D_2O. Longitudinal relaxation rates were measured using a nonselective inversion−recovery pulse sequence, and T_1 values were obtained from a three-parameter fit of the data to an exponential recovery function. ^{1}H−^{1}H-COSY and ^{1}H−^{13}C-HMQC spectra were recorded in magnitude mode using 256 increments and recycle delays optimized for fast-relaxing species.

Calculations and Computational Details. Multilinear least-squares fits with the one-nucleus method (eqs 5, 21) were performed with Microsoft EXCEL software. The best least-squares planes according to the three-nuclei method (eq 12) were obtained by minimizing M where M is the sum along the lanthanide series (j = 1 to 9 corresponding to Ln = Pr, Nd, Eu, Tb, Dy, Ho, Er, Tm, Yb) of the square of the orthogonal distances to the plane.[35] As a plane is defined by its distance to the origin and by its unit normal, $\vec{n}$, we add to M the following condition: $\varphi = (\vec{n}\cdot\vec{n}) - 1 = 0$ multiplied by a so-called Lagrangian multiplier λ.[36] After equating all the partial derivatives with respect to n_x, n_y, n_z, and λ to zero, a system of equations is found which can be solved by using a software for symbolic computation,[37] thus leading to the best least-squares plane.

Acknowledgment. This work is supported through grants from the Swiss National Science Foundation and by the Commissariat à l'Energie Atomique, Direction de l'Energie Nucléaire.

Supporting Information Available: Table S1 detailing longitudinal relaxation times obtained for the complexes $[Lu_xLn_{3-x}(TACI\text{-}3H)_2(H_2O)_6]^{3+}$. Figures showing correlations according to the one-nucleus method (eqs 10, 11, Figures S3 and S6), to the two-nuclei method (eq 8, Figures S1), and to the three-nuclei method (eq 12, Figure S4) for the complexes $[Lu_xLn_{3-x}(TACI\text{-}3H)_2(H_2O)_6]^{3+}$. Figure S2 displaying plots of $1/T_{1_i}^{para}$ vs $\sum_{m=1}^{2}(r_i^m)^{-6}$ according to eq 22 and Figure S5 showing the plot of B_{ikl}^{exp} vs B_{ikl}^{calc} for $[Ln_2Lu(TACI\text{-}3H)_2(H_2O)_6]^{3+}$. This material is available free of charge via the Internet at http://pubs.acs.org.

IC035093A

(35) Schomaker, V.; Waser, J.; Marsh, R. E.; Bergman, G. *Acta Crystallogr.* **1959**, *12*, 600.
(36) (a) Spiegel, M. R. *Advanced Calculus*, 5th ed.; Schaum's outline series; McGraw-Hill: New York, 1974; Chapter 8, pp 164, 171−174. (b) Atkins, P. W. *Physical Chemistry*; Oxford University Press: Oxford, 1994; pp A35−A36.
(37) *Maple 8*; Waterloo Maple Inc.: Waterloo, ON; www.maplesoft.com.